Master's Thesis

An Experimental and Numerical Study of Buoyancy Effect on the Flame Stability in Nonpremixed Laminar Coflow-jets

Suhyeon Oh

Department of Mechanical Engineering

Ulsan National Institute of Science and Technology

2021

An Experimental and Numerical Study of Buoyancy Effect on the Flame Stability in Nonpremixed Laminar Coflow-jets

Suhyeon Oh

Department of Mechanical Engineering

Ulsan National Institute of Science and Technology

An Experimental and Numerical Study of Buoyancy Effect on the Flame Stability in Nonpremixed Laminar Coflow-jets

A thesis/dissertation submitted to

Ulsan National Institute of Science and Technology

in partial fulfillment of the

requirements for the degree of

Master of Science

Suhyeon Oh

06. 16. 2021 of submission

Approved by

Advisor

Chun Sang Yoo

An Experimental and Numerical Study of Buoyancy Effect on the Flame Stability in Nonpremixed Laminar Coflow-jets

Suhyeon Oh

This certifies that the thesis/dissertation of Suhyeon Oh is approved.

06. 16. 2021 of submission

Signature

Advisor: Chun Sang Yoo

Signature

Jae Hwa Lee

Signature

Jooha Kim

To my husband, Kyu Ho.

Abstract

Based on the jet similarity solution of lifted flame, overall flame behaviors are investigated by varying the Schmidt number of fuel, Sc_F, with N_2, He, and Ar. For methane flames diluted with N_2, Ar, and He, nozzle-attached (Sc_F = 0.698), monotonically increasing lifted, non-monotonic lifted ($0.709 \leq Sc_F \leq 0.748$), and oscillating flames ($0.698 < Sc_F < 0.709$) are observed. Based on the results, the effects of Sc_F are further investigated by adding diluents such as N_2, Ar, and He to the methane/ethane fuel jet. In terms of Sc_F and fuel density, there were a first critical Schmidt number, $Sc_{F,cr1}$ from the boundaries of monotonically increasing flames and a second critical Schmidt number, $Sc_{F,cr2}$ for the decreasing and increasing liftoff height, H_L (U-shaped behavior). It had to do with the density differences of fuel, air, and burnt gas for the oscillating and stationary lifted flames. In the case of the increasing H_L (including the increasing regime in U-shaped behavior), H_L behaviors were correlated in terms of Sc_F, the density difference between fuel and air, $Sc_{F,cr1}$, and U_0. On the other hand, the decreasing H_L regime in the U-shaped behavior can be characterized with Sc_F and/or the Richardson number (defined by the density difference between fuel and air). Oscillating flames were observed by the repetitive action of positive $(\rho_{co}$ - $\rho_b)$ and negative $(\rho_F - \rho_{co})$ buoyancies. To further elaborate the characteristics of the oscillating lifted flames, experiments and numerical simulations were conducted by varying both fuel density (by varying propane and n -butane mixtures) and coflow density (by diluting air with N_2/He mixtures). Two different lifted flame oscillation behaviors are observed depending on these parameters: oscillating tribrachial lifted flame (OTLF) and oscillating mode-change lifted flame (OMLF), where a rapid increase in flame radius is observed. The regimes of the two flames are identified from experiments, which shows that OMLF occurs only when the effect of the negative buoyancy on the flow field by the fuel heavier than air becomes significant at low fuel jet velocity. OMLFs are also identified to distinguish OTLF regime from flame extinction, which implies that an OMLF can be extinguished when the positive buoyancy becomes weak, losing its stabilizing effect, or when the negative buoyancy becomes strong, further enhancing its destabilizing effect. Transient numerical simulations of both OTLF and OMLF reveal that the OMLF occurs by a strong toroidal vortex and a subsequent counterflow-like structure induced by relatively strong negative buoyancy. Such a drastic flow redirection significantly changes the fuel concentration gradient such that the OMLF changes its mode from a tribrachial flame mode (decreasing edge speed with fuel concentration gradient) to the premixed flame-like transition mode when the fuel concentration gradient becomes very small (increasing edge speed with fuel concentration gradient). Again, a tribrachial flame mode is recovered during a rising period of flame edge and repeats an oscillation cycle.

Contents

List of Figures

List of Tables

I Introduction

As international environment regulations have been tightened, it becomes inevitable to secure a combustion technology for near-zero emission on global market. Especially, many industries have decreased NO_x emission by recirculating exhaust gas released from a combustor. Unfortunately, however, it causes the reduction of thermal efficiency because the exhaust gas recirculation (EGR) requires an additional system from the outside to the inside. Therefore, multiple applications for an interior and induced recirculation system and fundamental characteristics of combustion should be accomplished.

The laminar flamelet model [3–5] has been extensively studied for the analysis of turbulent flames that consist of an ensemble of laminar flames. Now it is widely used for the design of industrial burners to increase the energy efficiency while decreasing NO_x emission. Especially, understanding of flame instability such as flame oscillation and extinction is one of the most important design factors to avoid the damage of the combustor and decrease the pollutant emission.

A laminar lifted jet flame usually exhibits a tribrachial (or triple) flame structure consisting of lean and rich premixed flame wings and a trailing diffusion flame inbetween, all of which originate from the tribrachial edge [1, 2, 6–9], as shown in Fig. 1. Since the tribrachial flame edge propagates towards unburnt mixture along the stoichiometric mixture isoline, the lifted jet flame stabilizes where its edge propagation speed, S_e, is balanced with local flow velocity, U_L [7, 8]. S_e is generally affected by mixture concentration gradient, mixture strength, flame curvature, and Lewis number, while U_L by jet momentum, flow redirection, and buoyancy. If even one of such flame and flow characteristics is changed, the lifted flame moves to another stabilization point or could start to oscillate [7, 8, 10–21].

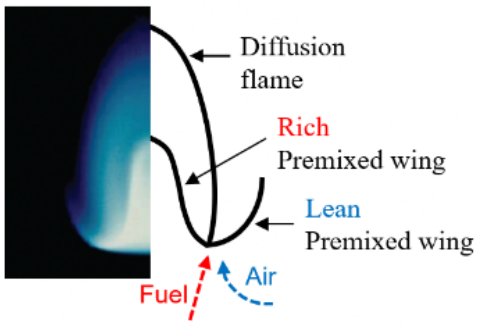

Figure 1: Direct image (left) [1] and schematic (right) of a tribrachial flame.

1.1 Jet similarity based on the cold jet theory

Chung and Lee [1, 6] proposed a theoretical equation that relates the liftoff height of a laminar lifted jet flame, H_L, with the fuel jet velocity, U_0, based on the cold jet theory [9, 22], and then, examined its validity through many experiments by varying the fuel type and the diameter and velocity of the fuel jets. Since the preheat zone of the lifted jet flame is usually less than 1 mm, it is readily assumed that the jet flow between the fuel nozzle exit and the flamebase of the lifted jet flame follows the cold jet theory by

ignoring the effect of gas expansion. For an axisymmetric steady laminar fuel jet, the similarity solutions are given by [1, 6, 23]:

$$u = \frac{3}{8\pi\nu x}\frac{J}{\rho}\frac{1}{(1+\eta^2/8)^2}, \tag{1}$$

$$Y_{\mathrm{F}} = \frac{(2Sc_{\mathrm{F}}+1)}{8\pi\nu x}\frac{I_{\mathrm{F}}}{\rho}\frac{2}{(1+\eta^2/8)^{2Sc_{\mathrm{F}}}}, \tag{2}$$

where η is the similarity variable defined as $\sqrt{u_{\mathrm{CL}}x/\nu}(r/x)$, u_{CL} is the centerline velocity $(3/8\pi)(J/\rho\nu)/x$, x is the axial coordinate, ν is the kinematic viscosity, J is the momentum flux $(\pi\rho U_0^2 d^2)/(3+j)$, I_{F} is the fuel mass flow rate $(\pi\rho U_0 Y_{\mathrm{F},0})/4$, Sc_{F} is the Schmidt number of fuel (ν/D_{F}), D_{F} is the mass diffusivity of fuel, and the subscript 0 indicates the condition at the nozzle exit. Here, j is 0 for the Poiseuille flow and 1 for uniform flow conditions at the nozzle exit.

A stationary lifted flame is stabilized at $\eta^*(x^*, r^*)$, where $Y_{\mathrm{F}} = Y_{\mathrm{F,st}}$ and $u = S_{\mathrm{e}}$. The liftoff height $H_{\mathrm{L}} = x^*$ and the limitation on jet velocity can be derived from Eq. 1 as follows:

$$\frac{H_{\mathrm{L}}}{d^2}\frac{\nu}{S_{\mathrm{e}}} = \left(\frac{3}{32}\right)\left(\frac{3}{2Sc_{\mathrm{F}}+1}\frac{Y_{\mathrm{F,st}}}{Y_{\mathrm{F},0}}\right)^{1/(Sc_{\mathrm{F}}-1)}\left(\frac{U_0}{S_{\mathrm{e}}}\right)^{(2Sc_{\mathrm{F}}-1)/(Sc_{\mathrm{F}}-1)}, \tag{3}$$

$$\frac{\eta^{*2}}{8} = \left(\frac{3}{2Sc_{\mathrm{F}}+1}\frac{Y_{\mathrm{F,st}}}{Y_{\mathrm{F},0}}\frac{U_0}{S_{\mathrm{e}}}\right)^{-1/2(Sc_{\mathrm{F}}-1)} - 1. \tag{4}$$

With the assumptions of constant S_{e} and $Y_{\mathrm{F,st}}$, the liftoff height relation becomes:

$$\frac{H_{\mathrm{L}}}{d^2}Y_{\mathrm{F},0}^{1/(Sc_{\mathrm{F}}-1)} = \mathrm{const}\times U_0^{(2Sc_{\mathrm{F}}-1)/(Sc_{\mathrm{F}}-1)}. \tag{5}$$

Equation 5 explains that the liftoff height increases with U_0 for $Sc_{\mathrm{F}} > 1$ and $Sc_{\mathrm{F}} < 0.5$, while it decreases for $0.5 < Sc_{\mathrm{F}} < 1$. Based on the range of Sc_{F} by jet similarity solution, the experiments [1,6] showed that the pure fuel jets of propane with $Sc_{\mathrm{F}} = 1.37$ and *n*-butane with $Sc_{\mathrm{F}} = 1.52$ have a liftoff flame at certain U_0, while the pure methane and ethane flames, of which Sc_{F} are typically 0.70 and 1.06, respectively, are blown out directly from nozzle-attached flames. From the studies [1, 6], it was elucidated theoretically and experimentally that the lifted flames of methane and ethane are immediately blown off once they are lifted off from the fuel jet nozzle by large jet velocity. Likewise, unlike the results of jet similarity, the hydrogen jet flame with $Sc_{\mathrm{F}} < 0.5$ keeps being nozzle-attached even when U_0 becomes comparable to the speed of sound [6]. This is primarily attributed to the strong mass diffusion of hydrogen that induces a negative quenching distance, H_{q}, from the nozzle tip [6].

1.2 Stabilization mechanism

As predicted from the similarity solution for the axisymmetric steady laminar jet, stationary lifted flames for propane and *n*-butane fuel jets, the blowoff directly from attached flames for methane and ethane fuel jets, and nozzle-attached flames for hydrogen fuel jets even at 10^3 m/s were observed from the experiments [1,6,23]. Chung [2] proposed a phenomenological explanation on the stabilization mechanism of a lifted jet flame through the kinematic behavior of its flame edge for different Sc_F.

Figure 2 shows the schematic of the stoichiometric isolines and the iso-velocity lines of S_e, where the stabilization points are located at closed circles [2]. With the assumption of constant S_e [1], the stability can be adjusted by perturbing the edge along the stoichiometric contour, $Y_{F,st}$. For $Sc_F > 1$, if the edge is perturbed downstream (upstream) of the stabilization point, the flow velocity becomes lower (higher) than the constant S_e. Thus, the edge will move back to the stabilization point, thereby being stable. On the other hand, for $Sc_F < 1$, the stoichiometric isoline crosses the iso-velocity line from the outside due to $\nu < D_F$. For that reason, the edge between the nozzle exit ($x = 0$) and the stabilization point is under a relatively small momentum in the axial direction, while the edge beyond the stabilization point has a certain effect of axial momentum, which causes the instability of the flame. For $Sc_F < 0.5$, the stoichiometric isoline diverges near the upstream, implying strong mass diffusion to the nozzle exit. In experiments, a nozzle-attached flame can survive high jet velocity up to the speed of sound: for instance, the hydrogen jet flame survives as an nozzle-attached flame even at 1320 m/s.

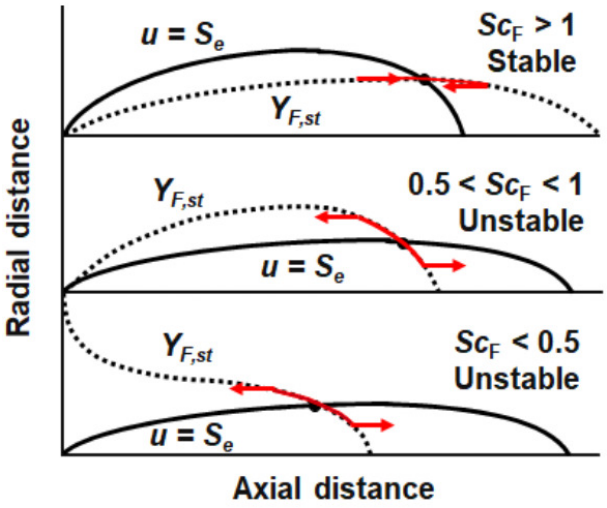

Figure 2: Schematic of stability of lifted flames with Schmidt number in free jets [2]. Dotted and solid lines represent the iso-concentration of stoichiometry and iso-velocity of S_e, respectively.

Besides the effect of the Schmidt number of the fuel jet, Sc_F, on the stabilization of the lifted jet flame, the buoyancy effect has been also widely investigated [15,18]. Won et al. [15] observed stationary lifted flames of even CH_4/N_2 jets in coflow, of which $Sc_F < 1$, elucidating that the buoyancy plays a

critical role in stabilizing the lifted flame by modifying flow field. In addition, Van et al. [18] recently reported the strange behavior of a stationary lifted flames of CH_4/N_2 jets that H_L decreases and then increases with increasing jet momentum, although it is supposed to increase with increasing the jet momentum, which is called a U-shaped behavior of the lifted flame. It was conjectured to occur because the effect of buoyancy over convection becomes strong at relatively-small jet velocities.

1.3 Oscillating mechanism: Competition between positive and negative buoyancies

The effect of buoyancy has been considered as one of the major factors to oscillate a lifted flame. Won et al. [14] observed oscillating lifted flames of nitrogen-diluted propane jets in coflow, which was identified to be induced by buoyancy from microgravity experiments. Recently, Van et al. [19] found that such flame oscillation occurs primarily due to competition between the positive buoyancy induced by burnt gas and the negative buoyancy by fuel, especially heavier than coflow. Noting that the flame volume was time-dependent during the oscillation, the positive buoyancy, $(\rho_{co}$ - $\rho_b)$ and the negative buoyancy, $(\rho_F - \rho_{co})$ were defined in terms of densities, where ρ_F and ρ_b are the densities of fuel stream and burnt gas, respectively. The negative buoyancy decreases the upstream velocity by directing fuel stream heavier than coflow air toward upstream, and then initiates flame oscillation; on the contrary the positive buoyancy increases flow velocity upstream of the flame by entraining coflow and consequently push the flame downstream. The competition between two counteracting buoyancies contributes to the complete cycle of the flame oscillation.

Even though previous studies have provided a new insight on the role of buoyancy in destabilizing the lifted flames, it still requires to further investigate the buoyancy effects on the liftoff height variation and oscillation characteristics of the lifted flames. In this study, we experimentally measure the total behaviors of lifted flames by adding diluents such as He, Ar, and N_2 to the fuel jet to control Sc_F. In addition, we investigate the oscillating mechanism of lifted flames experimentally and numerically, focusing on the structure change in two different oscillating flames: one retains the tribrachial flame behavior while oscillating, and the other keeps changing its characteristic flame shape.

In Chapter II, we introduce experimental and numerical setups for measuring and simulating lifted flames, which is then followed by the overall explanation of the overall characteristics of stationary and oscillating lifted flames in Chapter III. In Chapter IV, we classify stable lifted flames into several different regimes by characterizing H_L and buoyancies while for oscillating flames, we investigate the structural change of oscillating flames in terms of flame speed and fuel concentration gradient. This dissertation consists of materials that have been previously published in journals:

- S. Oh, K. H. Van, K. S. Jung, C. S. Yoo, M. S. Cha, S. H. Chung, and J. Park, "On the characteristics of oscillating lifted flames in nonpremixed laminar coflow jets: An experimental and numerical study", *Proc. Combust. Inst.* vol. 38, pp. 2049-2056, 2021.
- K. H. Van, S. Oh, C. S. Yoo, J. Park, and S. H. Chung,"Effects of Schmidt number on non-monotonic liftoff height behavior in coflow-jet flames with diluted methane and ethylene", *Proc. Combust. Inst.* vol. 38, pp. 1913-1921, 2021.

II Experimental and Numerical Methods

2.1 Experimental setups

The experimental apparatus consists of a coflow burner, a flow control system, and measurement setups. Because we need to significantly decrease the jet momentum to further investigate the structural change of the oscillating flames near extinction limit, two types of burners are used for a stable lifted flame and an oscillating flame.

The burner for a stable lifted flame includes a fuel nozzle with 4 mm inner diameter, d and 600 mm length to attain fully developed velocity profile, and a cylindrical quartz tube with 93 mm inner diameter. To ensure a uniform flow at the coflow exit, a layer of glass beads and a ceramic honeycomb are installed at the bottom of the coflow section and near the exit of the nozzle, respectively. An acrylic cylinder is placed on the coflow nozzle having four rectangular quartz windows for measuring lifted flames and preventing ambient air entrainment. Similarly, a fuel jet in the burner for an oscillating flame issues from a fuel nozzle with 10.7 mm inner diameter, d, and 850 mm length, L. The fuel jet velocity, U_0 varies in a range of $3 \leq U_0 \leq 12$ cm/s to find oscillating lifted flames. The fuel is surrounded by coflow issuing through a cylinder (150 mm i.d. and 600 mm length). Commercially-pure grade gases ($> 99.95\%$) are used for the experiments. To mix fuel and oxidizer with diluents, two mixing chambers are installed for the streams, of which flow rates are controlled by flow controllers with 99% accuracy. The lifted flames are measured using a digital camera (300 fps) attached to a two-axis translation stage. The flame edge location in the radial and vertical directions, (R_L, H_L), of a lifted flame is defined as the brightest locus in a converted gray-scale image. Figure 3 shows the schematic of the experimental setups to measure the behaviors of lifted flames.

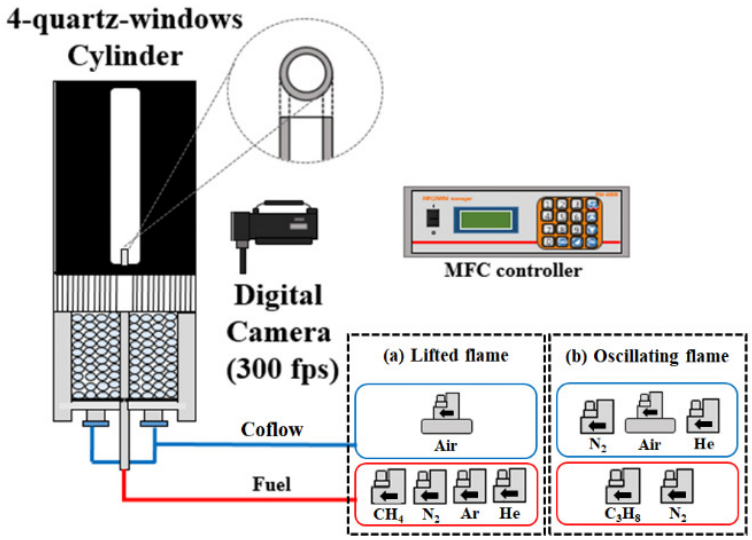

Figure 3: Schematic of experimental setups for (a) lifted flame and (b) oscillating flame.

Table 1 lists the test conditions for fuel jet composition with diluents of N_2, He, Ar and corresponding density and fuel Schmidt number. For methane jets, the mole fraction of fuel is fixed at $X_{CH_4} = 0.3$ and $X_i = 0.7$ (i = He, N_2, Ar and their mixtures), yielding the Schmidt number range of 0.698 to 0.871. To further investigate the effect of Sc_F on liftoff height, methane and ethylene mixture fuels are tested.

Table 1: Experimental conditions in the burner for stable lifted flame.

Fuel	X_F	ρ_F [kg/m^3]	T_{ad} [K]	Sc_F	ν [cm^2/s]	D_F [cm^2/s]
CH_4	0.300	0.31 ($X_{He} = 0.70$) - 1.33 (X_{Ar}=0.70)	1980 - 2080 (2020 at X_{He}= 0.35)	0.698 (X_{Ar}= 0.70) - 0.871 ($X_{He} = 0.70$)	0.157 (X_{Ar}= 0.70) - 0.196 ($X_{He} = 0.70$)	0.225
CH_4+C_2H_4 (3:1)	0.230	0.30 - 1.43	1980 - 2100	0.742 - 0.967	0.155 - 0.202	0.209
CH_4+C_2H_4 (1:1)	0.185	0.30 - 1.49	1970 - 2100	0.793 - 1.078	0.153 - 0.208	0.193
CH_4+C_2H_4 (1:3)	0.155	0.30 - 1.53	1970 - 2110	0.853 - 1.198	0.151 - 0.212	0.177
C_2H_4	0.135	0.29 - 1.56	1970 - 2120	0.932 - 1.335	0.150 - 0.215	0.161

Table 2: Experimental conditions in the burner for oscillating flame.

Fuel	X_F	ρ_F [kg/m^3]	ρ_{co} [kg/m^3]	T_{ad} [K]
C_3H_8	0.13	1.223	1.046 (X_{He}=1) - 1.168 (X_{He}=0)	1870 - 1940
	0.14	1.230		1890 - 1960
	0.15	1.236		1910 - 1980
	0.16	1.242		1930 - 2000
	0.17	1.249		1940 - 2010
C_3H_8+n-C_4H_{10} (3:1)	0.12	1.233		1870 - 1940
	0.13	1.241		1890 - 1960
	0.14	1.249		1910 - 1980
	0.15	1.257		1930 - 2000
	0.16	1.265		1940 - 2010

As shown in Table 2, the fuel in the burner for oscillating flame is propane or propane/n-butane mixture diluted with N_2, for which the fuel mole fraction, X_F, varies from 0.12 to 0.17. The coflow is air diluted with N_2/He mixture such that its density, ρ_{co}, can be controlled by varying the mole fractions of

N_2 and He (X_{N_2}) and X_{He}), while X_{N_2}+X_{He} = 0.125. Binary fuel mixture of propane/*n*-butane was tested to further investigate the effect of fuel density on oscillating flame behavior.

We used the Chemkin Pro package [24] with GRI 3.0 Mech [25] to maintain the Tad having a similar range as that for the methane (propane) flames in the burner for stable lifted (oscillating) flame by adjusting the fuel mole fraction. The transport properties such as kinetic viscosity, ν, and fuel mass diffusivity into air stream, D_F, are calculated from an open-source program [26] to determine $Sc_F = \nu/D_F$. The effective diffusivity of mixture fuel of methane and ethylene was determined from $D_F = X_{CH_4}D_{CH_4} + X_{C_2H_4}D_{C_2H_4}$ [27].

2.2 Numerical methods

For simulations of two different modes of oscillating flames, time-dependent, 2-D axisymmetric governing equations in the cylindrical coordinates (r,x) are solved using the laminarSMOKE [28, 29] code based on OpenFOAM [30]. Figure 4 shows a schematic of the computational domain. The main domain size is $R_0 \times L_z$ = 7.5 cm $\times$ 10 cm in the *r*- and *z*- directions, respectively. The inner radius of the fuel tube is 0.535 cm and its thickness is 0.078 cm. A uniform grid resolution of 100 μm is used for the simulations. Since the flame thickness is found to be approximately 1.1 mm, such grid resolution is fine enough to capture the flame structure and dynamics.

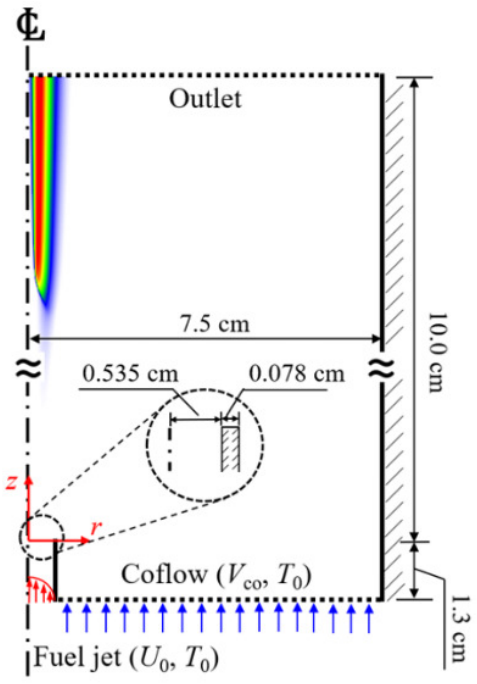

Figure 4: Schematic of numerical domain for simulations of oscillating lifted propane jet flames in helium-diluted coflow air.

For the fuel jet boundary condition, a fully-developed velocity profile of the Poiseuille flow is specified at 1.3 cm below the fuel nozzle exit while a uniform velocity profile is used for the oxidizer stream.

The fuel inlet velocity is specified as that of a fully developed pipe flow for which the mean velocity, U_0, is 6 cm/s, and the coflow velocity, V_{co}, is fixed to be 8 cm/s in accordance with the present experiment. For all the walls, no slip and non-permeable boundary conditions are used and isothermal boundary condition is employed in the fuel nozzle wall. At the outlet, zero-gradient outflow boundary condition is applied. Radiation is considered only for gas-phase with an optically-thin model [31]. A two-step global chemical mechanism of propane oxidation is adopted [32, 33].

III Overall characteristics of lifted flames

3.1 Stable lifted flame

Direct images of laminar coflow flames of methane diluted with N_2, Ar, and He are shown in Fig. 5 in terms of jet velocity at (X_{CH_4}, X_{N_2}, X_{He}, X_{Ar}) = (a) (0.3, 0, 0.7, 0), (b) (0.3, 0.7, 0, 0), and (c) (0.3, 0, 0, 0.7). With the He-dilution (Sc_F = 0.871), the liftoff height increases monotonically with the jet velocity (Fig. 5(a)), while the liftoff height exhibits a non-monotonic U-shaped behavior with the jet velocity (Fig. 5(b)) with the N_2-dilution (Sc_F = 0.714). The Ar-diluted flame (Sc_F = 0.698) is attached to the nozzle.

Although the sequential images are not represented in Fig. 5, the lifted flame for $0.698 < Sc_F < 0.709$ is not stationary and it oscillates for U_0 = 16 cm/s. The oscillation maintains up to U_0 = 20 cm/s and it becomes nozzle-attached at U_0 = 22 cm/s.

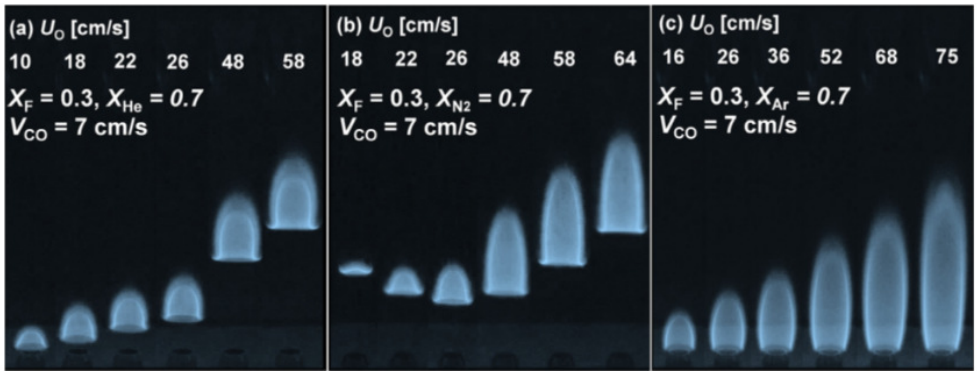

Figure 5: Direct images of typical lifted flames with U_0 for monotonically increased H_L in (a) helium-diluted methane, (b) U-shaped H_L in nitrogen-diluted methane, and (c) nozzle-attached flames in argon-diluted methane for X_F = 0.30 and V_{co} = 7 cm/s.

Variations in the liftoff height with increasing jet velocity at various Sc_F are plotted in Fig. 6 with X_{CH_4} = 0.3 for methane flames diluted with N_2, He, and Ar. The diluent volume fraction Ω_j in the fuel stream (N_2 mixed with He or Ar) is defined as $\Omega_j = X_j/((X_j + X_{N_2}))$ where j denotes He or Ar. Since X_{CH_4} = 0.3 and $X_j + X_{N_2} = 0.7$, Ω_{He} = 1.0 corresponds to X_{He} = 0.7 and X_{N_2} = 0 and Ω = 0 to N_2-dilution (X_{N_2} = 0.7). For comparison, the jet developing length Z_{free} by a free jet theory [34] is plotted with the black lines indicating the range of Z_{free}. Here, $Z_{free}/D = 0.0165 Re_D$. Thus, the axial distance $z < Z_{free}$ ($z > Z_{free}$) corresponds to the jet developing (developed) region.

For small jet velocities, the buoyancy effect exerted by burnt gas dominates over convection, which can be represented by the Richardson number $Ri \equiv (\rho_{co} - \rho_b)gd/\rho_F U_0^2$, where g is the gravitational acceleration. The range of Ri is marked in the orange lines. The result shows that the Richardson number decreases appreciably with the jet velocity, implying that the buoyancy effect can be significantly dominant on small jet velocities.

The results in Fig. 6 shows that the liftoff height with jet velocity exhibits the U-shaped behavior for

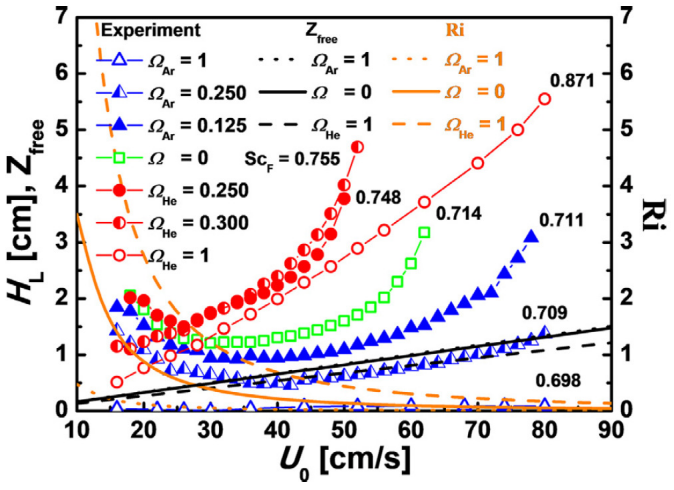

Figure 6: Variations in liftoff height with fuel jet velocity at various Schmidt numbers for methane flames diluted with N_2 and/or He or Ar.

$0.709 \leq Sc_F \leq 0.748$, nozzle-attached flame for $Sc_F = 0.698$, and monotonically increasing behavior for $Sc_F \geq 0.755$. This emphasizes the important roles of the Schmidt number and Richardson number on the liftoff height behavior. Although not indicated, the lifted flame oscillates for $0.698 < Sc_F < 0.709$. It results from Ar as the diluent, which is heavier than coflow air, implying that lifted flame could be influenced by a negative buoyancy exerted on fuel in the downward direction [19].

Recognizing the importance of fuel density, we further examine the overall behavior of lifted flame for methane diluted with N_2, He, and Ar in terms of the fuel Schmidt number and fuel density, and it will be discussed in Chapter IV.

3.2 Oscillating flame

Figure 7 shows sequential images of oscillating lifted flames of propane jet in helium-diluted coflow. Two types of oscillating flames are exhibited. First, the oscillating flame retains its tribrachial structure, exhibiting a typical near-sinusoidal behavior of the liftoff height, H_L. Second, the lifted flame keeps changing its flame structure, exhibiting a rapid increase in its radius near the bottom of oscillation of H_L. Hereafter, the former is named as oscillating tribrachial lifted flame (OTLF) and the latter oscillating mode-change lifted flame (OMLF).

When the OTLF propagates upstream towards the nozzle (Fig. 7a), the flame consumes the fuel accumulated between the nozzle and flame and its radial size, R_L, keeps increasing, which in turn maximizes the positive buoyancy and makes coflow entrainment large enough to push the flame edge downstream [19]. As it moves downstream, the fuel is accumulated and the flame size decreases, resulting in the decrease in the effect of the positive buoyancy and then starts to propagate upstream, completing an oscillation cycle. On the contrary, when the OMLF propagates upstream, its trailing diffusion flame gradually shrinks and its flame structure changes from a tribrachial (7b-I) to a premixed-like one (7b-II). Then, the flame edge rapidly propagates radially (7b-III) and finally recovers its tribrachial structure

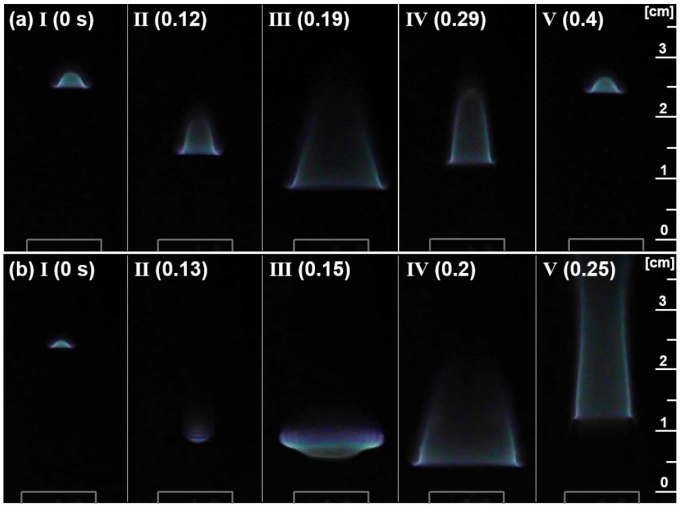

Figure 7: Direct images of (a) OTLF with $\rho_{co} = 1.155$ kg/m^3 and (b) OMLF with $\rho_{co} = 1.058$ kg/m^3 of propane jet in helium-diluted coflows with $X_F = 0.15$ (ρ_F = 1.236 kg/m^3), $U_0 = 4.5$ cm/s, and $V_{co} = 8$ cm/s. The oscillation frequencies are (a) 2.482 and (b) 2.503 Hz, respectively.

(7b-IV), and propagating downstream (7b-V), completing an oscillation cycle.

To elucidate the overall characteristics of OTLF and OMLF, we identify their regime diagram in the space of ρ_{co} and U_0 for various X_F as shown in Fig. 8. Since the characteristics of OTLF were discussed in detail previously [18], here we focus on OMLF. Several points are noted.

First, for all X_F, OMLF develops at relatively-low ρ_{co} and U_0 such that its regime lies at the lower-left corner of the OTLF regime. This implies that OMLF occurs only when the effect of the negative buoyancy by fuel on the flow field becomes significant (small ρ_{co}) at low U_0. Second, OMLF regime becomes the largest at X_F = 0.15 and nearly vanishes at X_F = 0.17. When X_F is further increased/decreased ($X_F \geq 0.18$ or $X_F \leq 0.13$), there exist no OMLFs (not shown here) because the corresponding flame strength is too high/low to induce OMLFs. As such, it is reasonable that OMLF regime is maximized at a certain X_F = 0.15. Third, there exist three extinction mechanisms for both OTLFs and OMLFs: for instance, from 0 to 1, 3, or 4 as illustrated in Fig. 8b. OTLF is extinguished when the positive buoyancy is decreased ($0 \rightarrow 1$) or the effect of the negative buoyancy becomes significant at low U_0 where the buoyancy overwhelms the fuel jet momentum ($0 \rightarrow 3$). OTLF can also be blown out by large U_0 ($0 \rightarrow 4$). However, OTLF can be stable when the positive buoyancy increases ($0 \rightarrow 2$) as discussed in [19].

To further elucidate the oscillation dynamics of OTLF and OMLF, we performed two-dimensional transient numerical simulations of both OTLF and OMLF of a nitrogen-diluted propane jet with X_F = 0.1 (ρ_F = 1.203 kg/m^3) in coflows with different ρ_{co} at U_0 = 6 cm/s: for the OTLF and OMLF, ρ_{co} are set to 1.125 and 1.041 kg/m^3, respectively. Figure 9 shows the temporal evolutions of OTLF and OMLF using the isocontours of heat release rate, q. The streamlines are also shown to identify the temporal evolutions of local flows while the isolines of CO_2 mass fraction, Y_{CO_2}, of 0.10 and ξ_{st} to identify their flame edges. Note that ξ_{st} are 0.283 and 0.298 for OTLF and OMLF, respectively, and Y_{CO_2} = 0.10 isoline approximately encompasses the maximum q, q_{max}. Several points are noted.

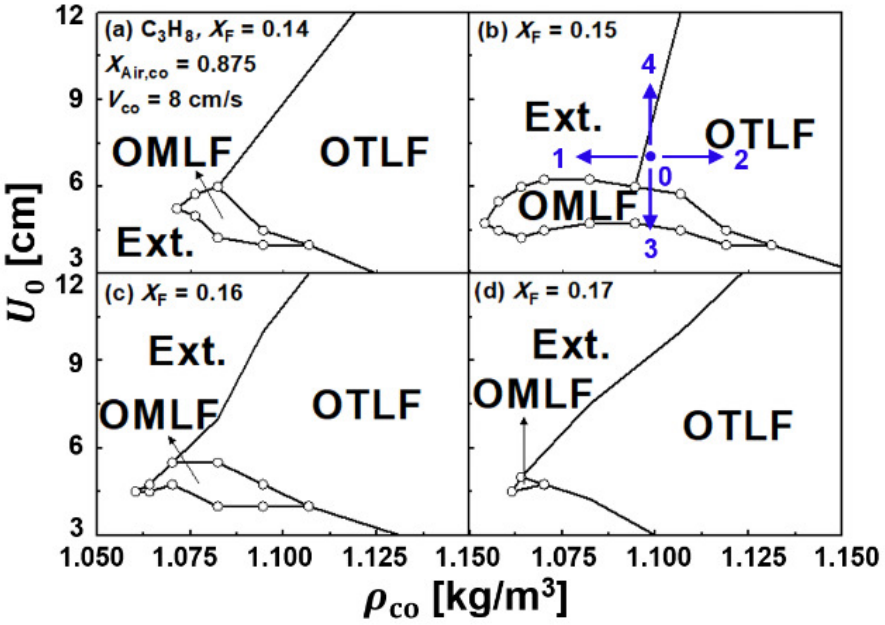

Figure 8: Regime diagram of OTLF and OMLF of propane jet in helium-diluted coflow in the space of the coflow density, ρ_{co}, and the fuel jet velocity, U_0, at $V_{co} = 8$ cm/s for (a) $X_F = 0.14$, (b) 0.15, (c) 0.16 and (d) 0.17.

First, it is readily observed from Fig. 9 that the oscillation characteristics of OMLF are different from those of OTLF, which is primarily attributed to the development of a toroidal vortex (9b-I) and resulting counterflow-like structure (9b-II) ahead of OMLF propagating upstream. Since there exist only ρ_{co} difference between the two oscillating flames, we can confirm that such flow structures are induced by a relatively-strong negative buoyancy ($\rho_F - \rho_{co}$) of the OMLF and consequently renders OMLF to move more radially outward than OTLF. Although the two-step global mechanism was used for this simulation, we founded OTLFs and OMLFs such that only flame dynamics was considered, not any chemical kinetics.

Second, for the OTLF vigorous heat is released near the flamebase or the tribrachial point during the whole cycle. For the OMLF, however, vigorous heat is first released over a wide area from the tribrachial point to the rich-premixed flame wing (9b-I and II), and is then concentrated at the tribrachial point (9b-IV and V). In addition, the trailing diffusion flame of OMLF is much weaker than that of OTLF especially when the OMLF propagates upstream and radially outward (9b-II and III), similar to the present and previous experimental results [19]. In Fig. 9b-II, there is a little bit of the heat release rate of the trailing diffusion flame. Since we focus on not a stationary flame but an oscillating one, the diffusion branch of the OMLF in the simulation cannot vanish totally even for the premixed-like flame. The evaluation about the premixed-like structure will be discussed later.

Third, for the OMLF q_{max} occurs in the rich-premixed flame wing when it propagates upstream by relatively-strong negative buoyancy, and hence, it becomes more like a premixed flame propagating in a stratified charge than a tribrachial flame (9b-II and III). After that, OMLF retains its tribrachial flame

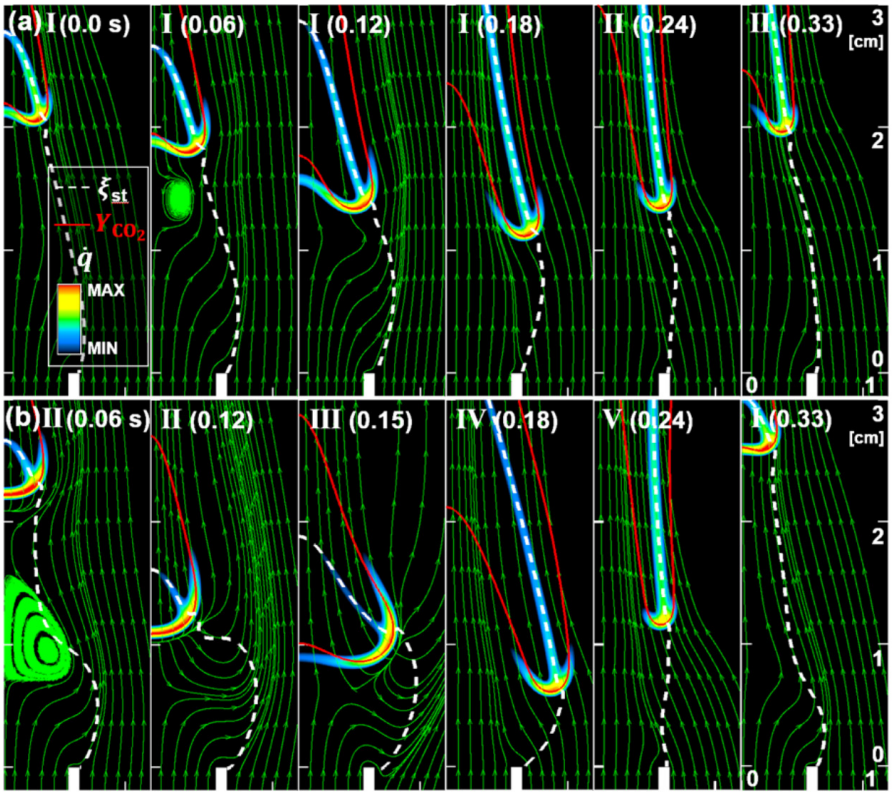

Figure 9: Temporal evolutions of (a) OTLF with ρ_{co} = 1.125 [kg/m^3] and (b) OMLF with ρ_{co} = 1.041 [kg/m^3] of nitrogen-diluted propane jet with X_F = 0.1 (ρ_F = 1.203 [kg/m^3]). Color contours and arrow lines represent heat release rate, q; and streamlines, respectively; solid and dashed lines represent the isolines of the stoichiometric mixture fraction, ξ_{st}, and CO_2 mass fraction, Y_{CO_2}, of 0.10. The oscillation frequency was (a) 2.857 and (b) 2.778 Hz, respectively.

structure while moving downstream.

As the previous work [19], we can confirm experimentally and numerically the effect of the two buoyancies on oscillating flame. In Chapter IV, we will analyze the relationship between the buoyancy and the flame structure in detail and introduce other parameters to explain the change of flame structure.

IV Buoyancy effect on H_L and structure of flame

4.1 The critical Sc_F on stable lifted flame

We further extended the range of fuel Schmidt number by using mixed fuels of CH_4 and C_2H_4. The range of Tad was adjusted by varying the fuel mole fraction X_F, so that the positive buoyancy exerted by burnt gas was kept nearly the same as that of methane fuel case.

Figure 10 shows overall regimes of flames with the various range of Sc_F in terms of the Schmidt number and fuel density. The behavior can be classified into three regimes: monotonically increasing behavior of liftoff height with jet velocity (regime I), U-shaped behavior (regime II), and flame oscillation (regime III). The solid line between regimes I and II (II and III) corresponds to the first (second) critical Schmidt number, $Sc_{F,cr1}$ ($Sc_{F,cr2}$), changing the lifted flame behavior for fixed fuel densities. The best fit correlation is $Sc_{F,cr1} = 0.22 + 0.72 \times \rho_F$ ($Sc_{F,cr2} = -6.79 + 6.73 \times \rho_F$) with R = 0.98 (0.91). The cross-point of $Sc_{F,cr1}$ and $Sc_{F,cr2}$ lines is 1.05, which is sufficiently close to unity, such that the U-shaped behavior can be observed for $Sc_F < 1$.

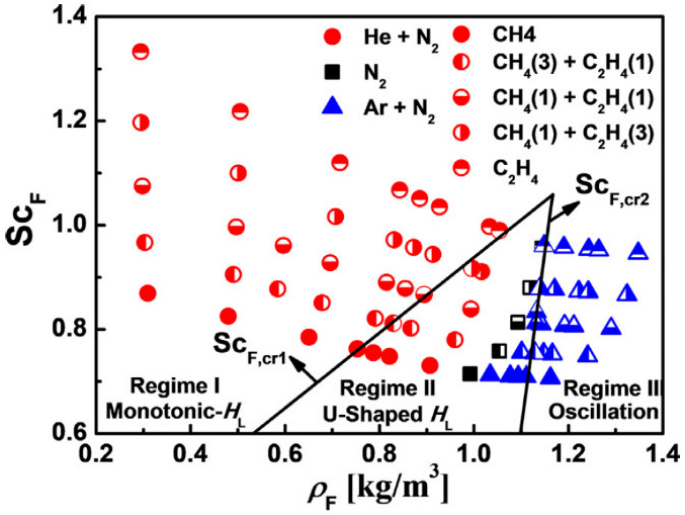

Figure 10: Regime diagram on lifted flame behavior in terms of fuel Schmidt number and fuel density. Fuel mole fractions were adjusted to keep the adiabatic flame temperature to be in the same range as those of methane fuel.

In regime I for $Sc_F > Sc_{F,cr1}$ with relatively small fuel density, jet momentum plays an important role for the stabilization of lifted flame such that the liftoff height increases with jet velocity. In regime II for $Sc_{F,cr2} < Sc_F < Sc_{F,cr1}$ with intermediate fuel density, the relative role of the buoyancy over convection in flame stabilization is important at small jet velocities, whereas the flame stabilization was controlled by jet momentum at large jet velocities [18], thus exhibiting the U-shaped behavior. In regime III for $Sc_F < Sc_{F,cr2}$ with large fuel density, the negative buoyancy by the fuel heavier than air plays an important role in triggering the flame oscillation [19]. In summary, as the fuel density increases (there by Ri) at

a specified Sc_F, the flame stabilization exhibited monotonic behavior (regime I) for small ρ_F, U-shape behavior for intermediate ρ_F, and flame oscillation for sufficiently large ρ_F (especially larger than air density). The U-shaped behavior can only be observed for $Sc_F < 1$. As Sc_F decreases, the range of ρ_F for U-shaped behavior extends.

The liftoff height behavior in regime I and increasing range in the U-shaped behavior is characterized based on the jet velocity U_0 scaled by stoichiometric laminar burning velocity S_L^0 according to the stabilization mechanism [1, 2, 6] and the density difference (ρ_{co} - ρ_F) inducing positive buoyancy (ρ_{co} being coflow air density), thereby increasing local flow speed and liftoff height. The result is shown in Fig. 11 in terms of $(\rho_{co} - \rho_F)/\rho_F$ and (U_0/S_L^0). The best-fit is $H_L = 0.16 + 4.99 \times [(\rho_{co} - \rho_F)/\rho_F \times (U_0/S_L^0) \times Sc_{F,cr1}]^{(5.29\times(Sc-0.5))}$ with R = 0.91. The exponent $(Sc_F - 0.5)$ was chosen, because for the fuel with $Sc_F < 1$, the liftoff height behaviors between the fuels having $Sc_F < 0.5$ and $Sc_F > 0.5$ are quite different based on the free jet theory [1, 2, 6]. This relation is valid only for $Sc_F > 0.5$ and $(\rho_{co} - \rho_F) > 0$. An exceptional case is for $\Omega_{He} = 1.0$, where the liftoff height decreased with the increase in the above correlation, as shown in Fig. 11. This may be attributed partly to differential diffusion effect of the very light molecule of He and large stoichiometric laminar burning velocity.

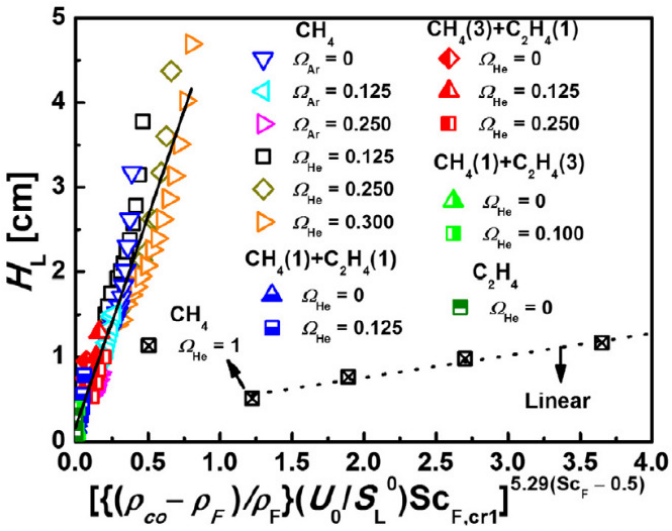

Figure 11: Characterization of increasing liftoff height behavior with jet velocity (increasing rage in U-shaped behavior is also included).

For the decreasing liftoff height with jet velocity in the U-shaped behavior, the relative role of the buoyancy over convection in flame stabilization was emphasized for small jet velocities [18]. For N_2-diluted methane flames, Sc_F varied from 0.710 to 0.714 (0.51% variation) while $(\rho_F - \rho_{co})$ varied 89%. As shown in Fig. 6, the density difference $(\rho_F - \rho_{co})$ influences appreciably on the liftoff height. Note that in the U-shaped regime, the difference $(\rho_F - \rho_{co})$ can be either positive or negative, as was shown in Fig. 12. Considering the importance of $(\rho_F - \rho_{co})$ and its sign, the liftoff height is correlated with a new Richardson number, $Ri \equiv |\rho_F - \rho_{co}|dg/\rho_F U_0^2$. Note that H_L decreases with the increase in Sc_F, which

has been explained previous by the competition between buoyancy-induced and jet momenta [19].

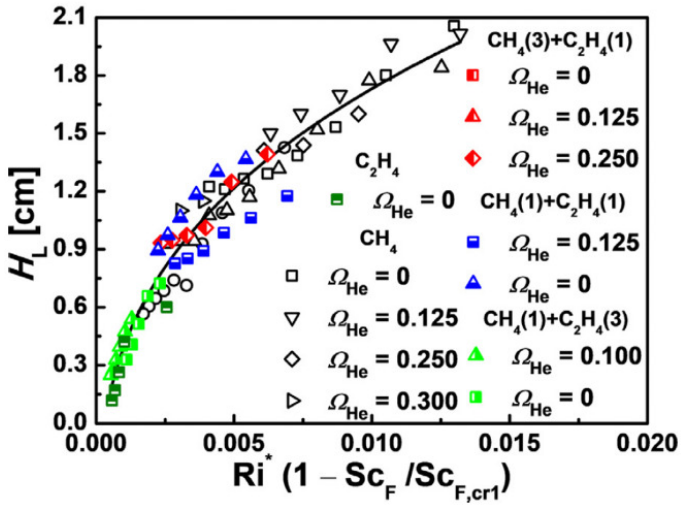

Figure 12: Characterization for decreasing liftoff height in U-shaped behavior, of which best fit is $H_L = -0.93 + 10.65 \times [Ri^*(1 - Sc_F/Sc_{F,cr1})]^{0.3}$ with R = 0.94.

The flame oscillation was previously shown to be attributed to the effects of competitive forces acting on the flow field by the positive buoyancy from burnt gas and negative buoyancy from the fuels, especially heavier than air (C_3H_8 and n-C_4H_{10}) [19], which corresponds to $Sc_F > 1$. Those critical onset conditions are marked as the dotted lines on Fig. 13 in terms of (ρ_{co} - ρ_b) and (ρ_F - ρ_{co}), demarcating the regions of stationary lifted flame, oscillation, and flame extinction regimes (ext1). These experimental data mainly with C_3H_8 and n-C_4H_{10} fuels corresponds to $(\rho_F - \rho_{co}) > 0.004$ kg/m^3 [19]. The range of $(\rho_F - \rho_{co})$ is appreciably extended (solid lines) for the present data by utilizing CH_4 and C_2H_4.

The present data in Fig. 13 were, for simplicity, taken with those of $Sc_{F,cr1}$ (data with black circles indicating U-shaped behavior) and $Sc_{F,cr2}$ (data with black triangles showing flame oscillation) along with flame conditions with the interval of 10% dilution ratio. The present data are represented as three shaded regions identified as monotonic increasing liftoff height behavior (regime I), U-shaped behavior (II), and flame oscillation (III). In the overlapped shades of regimes I and II, the data with black thick triangles correspond to regime II, otherwise regimes I. The solid line connecting the data of baselines case (X_{CH_4} = 0.3 and X_{N_2} = 0.7) near regimes I to II denotes extinction limit (ext2) such that the flame extinguishes (ext2) when (ρ_{co} - ρ_b) is reduced further, e.g., decreasing X_{CH_4} to 0.29 and X_{N_2} = 0.71, otherwise the flame shows a stationary lifted flame. Consequently, the map can be well explained by two parameters in Fig. 13: the density difference (ρ_{co} - ρ_b) representing the buoyancy due to burnt gas and the density difference (ρ_F - ρ_{co}) denoting the buoyancy due to fuel. Note that $(\rho_F - \rho_{co}) > 0$ results in a negative buoyancy on the cold coflow air, implying the downward direction of buoyancy force. While for $(\rho_{co} - \rho_b) > 0$, a positive buoyancy acts upwardly by the burnt gas.

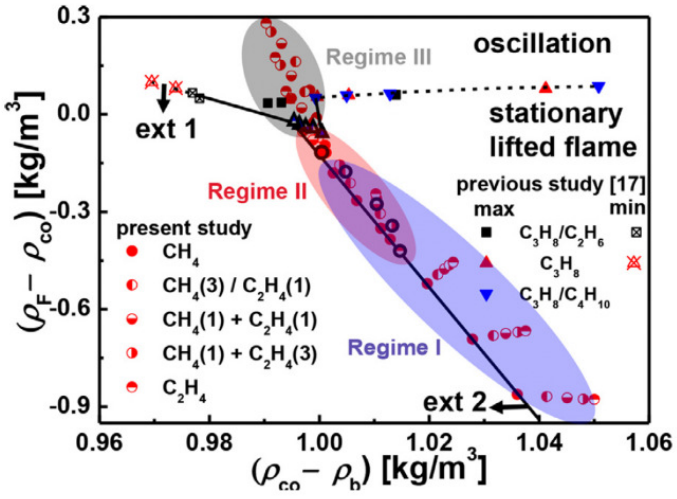

Figure 13: Critical onset conditions of flame oscillating and stationary lifted flame in terms of density differences (ρ_{co} - ρ_b) denoting positive buoyancy and (ρ_F - ρ_{co}) denoting negative buoyancy by fuel stream.

4.2 Flame propagation speed on oscillating flame

To further characterize OTLFs and OMLFs, the maximum and minimum ρ_{co} points of OMLF regimes in Fig. 8 and those of OTLF regimes are plotted in Fig. 14 in terms of the positive buoyancy $\sim (\rho_{co} - \rho_b)$ and the negative buoyancy $\sim (\rho_F - \rho_{co})$. The result shows that the regime of oscillating flames is distinguished from flame extinction by a straight line in the space of density differences, which implies that the extinction of an oscillating flame occurs when its positive or negative buoyancy is further decreased as discussed above and in [19].

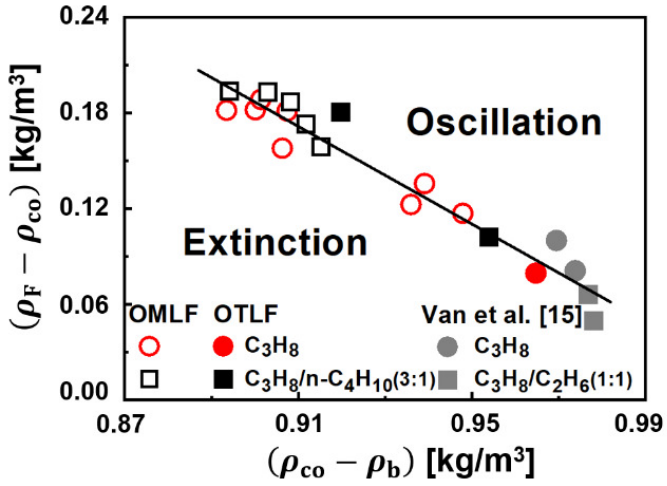

Figure 14: Boundaries of OTLFs and OMLFs in terms of (ρ_{co} - ρ_b) and (ρ_F - ρ_{co}).

Since both OTLF and OMLF boundaries are located on the same line, the characteristics of OMLFs

cannot be differentiated from those of OTLFs. Although Van et al. [18]'s oscillating flames are represented by gray, closed symbols, these include both OTLF and OMLF here because they didn't structurally divide the oscillating flames in their research. To explain the difference between two flames, we focus on velocities induced by the positive and negative buoyancies compared to U_0 and the laminar burning velocity, S_L^0, all of which influence flame oscillation characteristics. Note that the oscillation frequencies of OTLF and OMLF are almost same such that it is not considered as the oscillation parameter.(You can also know a little bit gap of frequency between two flames by simulations in Figs. 9and 16.) The present and previous experimental studies [19] show that as the negative buoyancy increases, a wider and stronger counterflow-like structure develops between the flame and nozzle, inducing a significantly-diverging flow redirection, which helps the oscillating flame to propagate upstream and radially outwards. On the contrary, as the positive buoyancy increases, coflow is more entrained into the flame, which pushes the oscillating flame downstream together with U_0.

Therefore, here we introduce two parameters to distinguish OMLFs from OTLFs. One is V^+/U_0, which represents the ratio of the characteristic velocity induced by the positive buoyancy to the fuel jet velocity:

$$V^+/U_0 = \sqrt{(\rho_{co} - \rho_b)gd/\rho_F}/U_0. \tag{6}$$

The other is V^-/S_L^0, which denotes the ratio of the characteristics velocity induced by the negative buoyancy to the laminar flame speed:

$$V^-/S_L^0 = \sqrt{(\rho_F - \rho_{co})gd/\rho_F}/S_L^0, \tag{7}$$

where g is the gravitational acceleration and d the nozzle inner diameter. S_L^0 is measured at the stoichiometric mixture fraction, ξ_{st}, evaluated from the mixture compositions of the fuel and oxidizer streams [35]. Note that V^+/U_0 represents the square root of the relative strength of the positive buoyancy to the fuel jet momentum, both of which push the flame downstream, while V^-/S_L^0 denotes that of the negative buoyancy to flame propagation or flame strength, both of which direct the flame upstream.

Figure 15 shows OMLFs in terms of V^+/U_0 and V^-/S_L^0. It is readily observed that OMLF data are aligned in a narrow region around the straight line marked, demonstrating that the OMLF regime sticks to the OTLF regime, separating the OTLFs from flame extinction regime. An OMLF can be extinguished when V^+/U_0 and/or V^-/S_L^0 decreases. This implies that an OMLF can be blown out when the positive buoyancy becomes relatively weak compared to U_0, and consequently loses its stabilizing effect. An OMLF can be also extinguished when the negative buoyancy becomes relatively strong compared to S_L^0, and further destabilizes it. Note that OMLFs of the propane/*n*-butane jet lie at relatively-large V^-/S_L^0 and relatively-small V^+/U_0 because its ρ_F is much larger than ρ_{co}.

To further identify the propagation characteristics of flames, we investigate their edge propagation speed,S_e, by evaluating the displacement speed, S_d. Since S_e is the relative displacement speed of a

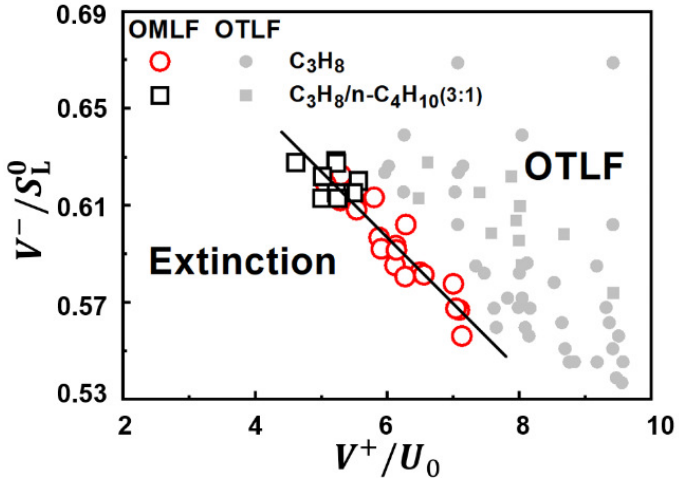

Figure 15: Oscillating mode-change lifted flames (OMLF) in terms of V^+/U_0 and V^-/S_L^0.

species mass fraction isocontour, S_e is obtained by calculating S_d at the flamebase, which is defined as [8, 36–40]:

$$S_e = S_d = \frac{1}{\rho|\nabla Y_k|}\left(\omega_k - \frac{\partial}{\partial x_j}(\rho Y_k V_{j,k})\right), \tag{8}$$

where Y_k is the mass fraction, $V_{j,k}$ the diffusion velocity in the j-direction, ω_k the net production rate of species k. In the present study, CO_2 is used for evaluating S_e. For both OTLF and OMLF, S_e is measured at the flamebase, which is defined as the intersection of the isolines of $Y_{CO_2} = 0.10$ and ξ_{st}.

Figure 16 shows the temporal evolutions of S_e and the local flow speed normal to the flamebase, U_N $(= \mathbf{u}\cdot\mathbf{n})$, for both oscillating flames, where $\mathbf{u}$ and $\mathbf{n}$ are the local flow velocity and the flame normal direction vector at the flamebase, respectively. In the figure, I∼II for the OTLF and I∼V for the OMLF correspond to the sequences of Figs. 9a and 9b. It is readily observed that for the OTLF, S_e becomes faster/slower than U_N in Regime I/Regime II, and hence, it propagates upstream in Regime I while it is pushed back downstream by large U_N in Regime II. For the OMLF, however, its dynamics becomes more complicated than that for the OTLF. Although overall S_e and U_N behave similarly to those of the OTLF, they exhibit larger amplitudes and mean values than those of the OTLF. In addition, S_e has several local peaks during the oscillation.

4.3 Fuel concentration gradient on oscillating flame

Since it is readily observed from Figs. 9 and 16 that S_e changes over time together with the size of the leading edge of the lifted flames, we investigate the effect of the fuel concentration gradient on S_e to further identify its characteristics for both oscillating flames. To facilitate understanding of the effect, a schematic of S_e of an edge flame with dY_F/dy in [2] is repeated in Fig. 17, where dY_F/dy represents the fuel concentration gradient, and Y_F and y are the fuel mass fraction and the tangential direction to the edge flame propagation, respectively. In general, S_e decreases with increasing dY_F/dy due to the

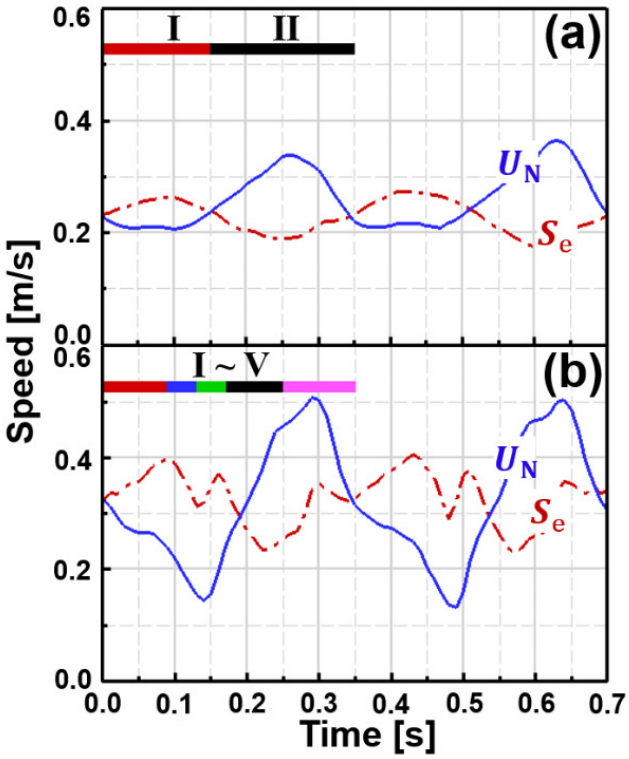

Figure 16: Temporal evolutions of edge propagation speed, S_e, and local flow speed normal to flame, U_N, at the flamebase for (a) OTLF and (b) OMLF. I $\sim$ II in (a) and I $\sim$ V in (b) represents the time sequences of the OTLF and OMLF in Fig. 6.

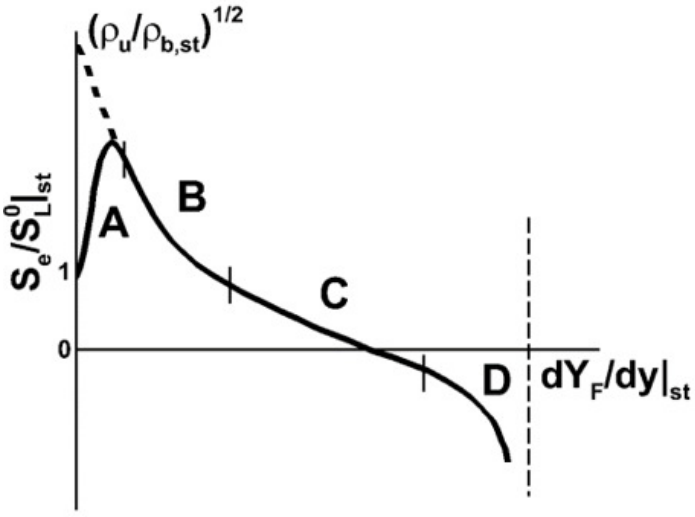

Figure 17: Schematic of edge flame propagation speed with the fuel concentration gradient (A, transition; B, tribrachial; C, bibrachial; D, monobrachial and near extinction regimes) from [2].

decrease of reaction intensity while its flame structure changes from a tribrachial (B) to a bibrachial (C) to a monobrachial flame (D). However, as dY_F/dy decreases and ultimately vanishes, S_e approaches the laminar burning velocity, S_L^0, due to the occurrence of transition (A) from a tribrachial flame to a premixed flame. As a result, S_e attains its maximum value between the transition and tribrachial edge flame regimes. For more details of the effect of dY_F/dy on S_e, readers are referred to [2].

Figure 18 shows the effect of dY_F/dy on S_e of the OTLF and OMLF, from which we can identify their oscillating dynamics in detail together with Fig. 9. As the OTLF propagates upstream towards the nozzle, flow divergence becomes large due to the negative buoyancy, which subsequently enlarges its radial size and decreases dY_F/dy, leading to an increase of S_e. As the OTLF further approaches the nozzle, both flame area and reaction intensity increase to entrain more coflow to the flame due to the positive buoyancy. Consequently, the OTLF starts to be pushed downstream by large U_N induced by the entrainment. However, as the OTLF moves downstream, flow divergence becomes small, which subsequently reduces its radial size and increases dY_F/dy, leading to a further decrease of S_e. As the OTLF moves further downstream, U_N becomes small and dY_F/dy increases again, leading to an increase of S_e. Then, the OTLF starts its oscillation again by propagating upstream. It is also identified from Figs. 6a and 9a that since the OTLF exhibits S_e inversely proportional to dY_F/dy regardless of its propagation direction (upstream or downstream) and maintains the tribrachial flame structure during its oscillation, it lies at the tribrachial flame regime (B) in Fig. 17.

For the OMLF, its cycle can be classified into five different regimes (Regimes I∼V) as shown in Figs. 9b and 18b. As the OMLF first propagates upstream, S_e increases due to the decrease of dY_F/dy (Regime I; the tribrachial flame regime (B) in Fig. 17), similar to the OTLF behavior. Meanwhile, a strong toroidal vortex is formed by relatively-large negative buoyancy, which subsequently induces a counterflow-like structure upstream of the flame (see Fig. 9b-II and III). This increases its leading edge

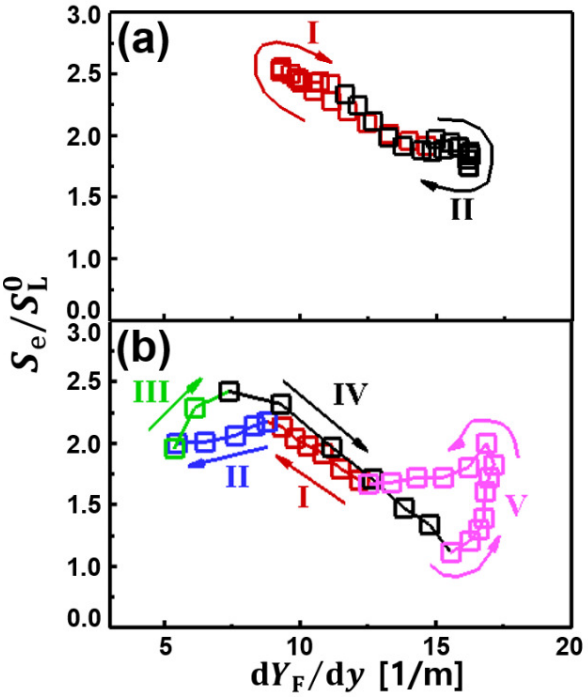

Figure 18: Variations of edge propagation speed, S_e, as a function of fuel mass fraction gradient tangential to the flamebase, dY_F/dy, for (a) OTLF and (b) OMLF. S_e is normalized by corresponding laminar burning velocity at stoichiometry, S_L^0.

size and decreases dY_F/dy, leading to a decrease of S_e with decreasing dY_F/dy (Regimes II and III; the premixed flame-like transition regime (A)). Such flow change consequently renders the OMLF to become more like a premixed flame in a stratified charge and to rapidly propagate radially outward. Meanwhile, the increase of flame area and reaction intensity by the radial flame propagation induces large coflow entrainment, which subsequently pushes the OMLF downstream, featuring a decrease of S_e with dY_F/dy (Regime IV; the tribrachial flame regime (B)). As the flame propagates further downstream, S_e is first increased significantly by an increase of the fuel concentration gradient normal to the flame edge propagation, dY_F/dn, rather than dY_F/dy due to positive buoyancy increase by breaking the counterflow-like structure and finally finishes its cycle by returning to its original starting point (Regime V). This causes the surge of S_e during the early stage of Regime V.

V Conclusion

We investigated behaviors of overall lifted flames by adding diluents to the fuel jets, thereby controlling the Schmidt number and buoyancy. At first, we experimentally investigated three different behaviors of lifted flames with different fuel Schmidt number with increasing jet velocity. Then, we conducted both experiments and numerical simulations to understand the characteristics of oscillating lifted jet flames.

In various ranges of the fuel Schmidt number, nozzle-attached, stationary lifted, and oscillating lifted flames were observed. Stationary lifted flames were classified as monotonic increasing and U-shaped flames with increasing jet velocity. For lifted flames, there existed the first critical Schmidt number ($Sc_{\mathrm{F,cr1}}$) below (over) which the monotonic increasing (U-shaped) behavior was exhibited. The second fuel Schmidt number ($Sc_{\mathrm{F,cr2}}$) existed over which the flame oscillated. Such cases ($Sc_{\mathrm{F}} < Sc_{\mathrm{F,cr2}}$) diluted with Ar resulted from the negative buoyancy by the heavier fuel stream than coflow air. The cross-point of the two critical Schmidt numbers represented $Sc_{\mathrm{F}} = 1.05$, which implies that the experimental results accord with the jet similarity solution because it is close to unity [1, 2, 6]. The dependencies of these critical Schmidt number were identified with $(\rho_{\mathrm{F}} - \rho_{\mathrm{co}})/\rho_{\mathrm{F}}$, U_0/S_{L}^0, and Ri based on $(\rho_{\mathrm{F}} - \rho_{\mathrm{co}})$.

From the regimes of the oscillating tribrachial lifted flame (OTLF) and the oscillating mode-change lifted flame (OMLF), the OMLF was found to occur only when the effect of the negative buoyancy on the flow field becomes significant at low U_0 such that the OMLF regime lies at the lower-left corner of the OTLF regime. It was also found that the OMLFs distinguish the OTLF regime from the flame extinction regime in the space of V^+/U_0 and V^-/S_{L}^0, implying that an OMLF can be extinguished when the positive buoyancy becomes weak compared to U_0, losing its stabilizing effect, or when the negative buoyancy becomes strong compared to S_{L}^0, further enhancing its destabilizing effect. From the transient numerical simulations of both OTLF and OMLF, it was found that the OMLF occurs when a strong toroidal vortex and a subsequent counterflow-like structure develop upstream of the flame by its relatively-strong negative buoyancy. Such a drastic flow redirection manipulates the fuel concentration gradient, the curvature of premixed wings and the propagation characteristics, thereby changing the flame mode. Therefore, the OMLF changes its mode from the tribrachial flame to the transition to again the tribrachial flame during an oscillation cycle.

References

[1] S. H. Chung and B. J. Lee, "On the characteristics of laminar lifted flames in a nonpremixed jet," *Combst. Flame*, vol. 86, pp. 62–72, 1991.

[2] S. H. Chung, "Stabilization, propagation and instability of tribrachial triple flames," *Proc. Combust. Inst*, vol. 31, pp. 877–892, 2007.

[3] N. Peters, "Laminar Diffusion Flamelet Models In Non-premixed Turbulent Combustion," *Prog. Energy Combust. Sci.*, vol. 10, pp. 319–339, 1984.

[4] D. Veynante and L. Vervisch., "Turbulent combustion modelling," *Prog. Energy Combust. Sci.*, vol. 28, pp. 193–266, 2002.

[5] H. Pitsch and N. Peters, "Unsteady Flamelet Modelling Of Turbulent Hydrogen-Air Diffusion Flames," *Symp. (Int.) Combust.*, vol. 27, pp. 1057–1064, 1998.

[6] B. J. Lee and S. H. Chung, "Stabilization of Lifted Tribrachial Flames in a Laminar Nonpremixed Jet," *Combst. Flame*, vol. 109, pp. 163–172, 1997.

[7] Y. S. Ko and S. H. Chung, "Propagation of unsteady tribrachial flames in laminar non-premixed jets," *Combst. Flame*, vol. 118, pp. 151–163, 1999.

[8] T. Echekki and J. H. Chen, "Structure and propagation of methanol-air triple flames," *Combust. Flame*, vol. 114, pp. 231–245, 1998.

[9] Y. Chen and R. W. Bilger, "Stabilization mechanisms of lifted laminar flames in axisymmetric jet flows," *Combust. Flame*, vol. 122, pp. 377–399, 2000.

[10] J. Buckmaster and M. Matalon, "Anomalous Lewis number effects in tribrachial flames," *Symp. (Int.) Combust.*, vol. 22, pp. 1527–1535, 1988.

[11] L. J. Hartely and J. W. Dold, "Stabilization of Lifted Tribrachial Flames in a Laminar Nonpremixed Jet," *Combust. Sci. Techol.*, vol. 80, pp. 23–46, 1991.

[12] G. R. Reutsch, L. Vervisch, and A. Liñán, "Effects of heat release on triple flames," *Phys. Fluids*, vol. 7, pp. 1447–1454, 1995.

[13] P. N. Kioni, B. Rogg, K. N. C. Bray, and A. Liñán, "Flame spread in laminar mixing layers: the triple flame," *Combst. Flame*, vol. 95, pp. 276–290, 1993.

[14] S. H. Won, J. Kim, M. K. Shin, S. H. Chung, O. Fujita, T. Mori, J. H. Choi, and K. Ito, "Normal and microgravity experiment of oscillating lifted flames in coflow," *Proc. Combust. Inst*, vol. 29, pp. 37–44, 2002.

[15] S. H. Won, J. Kim, K. J. Hong, M. S. Cha, and S. H. Chung, "Stabilization mechanism of lifted flame edge in the near field of coflow jets for diluted methane," *Proc. Combust. Inst.*, vol. 30, pp. 339–347, 2005.

[16] N. I. Kim, J. I. Seo, K. C. Oh, and H. D. Shin, "Lift-off characteristics of triple flame with concentration gradient," *Proc. Combust. Inst*, vol. 30, pp. 367–374, 2005.

[17] N. I. Kim, J. I. Seo, Y. T. Guahk, and H. D. Shin, "The propagation of tribrachial flames in a confined channel," *Combst. Flame*, vol. 146, pp. 168–179, 2006.

[18] K. Van, K. S. Jung, C. S. Yoo, S. Oh, B. J. Lee, M. S. Cha, J. Park, and S. H. Chung, "Decreasing liftoff height behavior in diluted laminar lifted methane jet flames," *Proc. Combust. Inst*, vol. 37, pp. 2005–2012, 2019.

[19] K. H. Van, J. Park, S. H. Yoon, S. H. Chung, and M. S. Cha, "Mechanism on oscillating lifted flames in nonpremixed laminar coflow jets," *Proc. Combust. Inst*, vol. 37, pp. 1997–2004, 2019.

[20] K. S. Jung, S. O. Kim, T. Lu, S. H. Chung, B. J. Lee, and C. S. Yoo, "Differential diffusion effect on the stabilization characteristics of autoignited laminar lifted methane/hydrogen jet flames in heated coflow air," *Combust. Flame*, vol. 198, pp. 305–319, 2018.

[21] K. S. Jung, B. R. Jung, S. H. Kang, S. H. Chung, and C. S. Yoo, "A numerical study of the pyrolysis effect on autoignited laminar lifted dimethyl ether jet flames in heated coflow air," *Combust. Flame*, vol. 209, pp. 225–238, 2019.

[22] O. Savaş and S. R. Gollahalli, "Stability of lifted flaminar round gas-jet flame," *J. Fluid Mech.*, vol. 165, pp. 297–318, 1986.

[23] B. J. Lee, M. S. Cha, and S. H. Chung, "Characteristics of Laminar Lifted Flames in a Partially Premixed Jet," *Combust. Sci. Technol.*, vol. 109, pp. 163–172, 1997.

[24] Ansys. Inc, "Chemkin-Pro 17.0," http://www.ansys.com.

[25] G. P. Smith, D. M. Golden, M. Frenklach, N. W. Moriarty, B. Eiteneer, M. Goldenberg, C. T. Bowman, R. K. Hanson, S. Song, W. C. J. Gardiner, V. V. Lissianski, and Z. Qin, "GRI-MECH 3.0," http://www.me.berkeley.edu/gri_mech/.

[26] D. S. Dandy, "Transport Properties Calculator," http://navier.engr.colostate.edu/index.html.

[27] F. Dinkelacker, B. Manickam, and S. P. R. Muppala, "Modelling and simulation of lean premixed turbulent methane/hydrogen/air flames with an effective Lewis number approach," *Combust. Flame*, vol. 158, pp. 1742–1749, 2011.

[28] A. Cuoci, A. Frassoldati, T. Faravelli, and E. Ranzi, "Numerical modeling of laminar flames with detailed kinetics based on the operator-splitting method," *Energy Fuels*, vol. 27, pp. 7730–7753, 2013.

[29] A. Cuoci, A. Frassoldati, T. Faravelli, and E.Ranzi, "A computational tool for the detailed kinetic modeling of laminar flames: Application to C_2H_4/CH_4 coflow flames," *Combust. Flame*, vol. 160, no. 5, pp. 870–886, 2013.

[30] H. G. Weller, G. Tabor, H. Jasak, and C. Fureby, "A tensorial approach to computational continuum mechanics using object-oriented techniques," *Comput. Phys.*, vol. 12, pp. 620–631, 1998.

[31] Y. Ju, H. Guo, K. Maruta, and F. Liu, "On the extinction limit and flammability limit of non-adiabatic stretched methane-air premixed flames," *J. Fluid Mech.*, vol. 342, pp. 315–334, 1997.

[32] M. Metghalchi and J. C. Keck, "Laminar burning velocity of propane-air mixtures at high temperature and pressure," *Combust. Flame*, vol. 38, pp. 143–154, 1980.

[33] R. Blint, "The relationship of the laminar flame width to flame speed," *Combust. Sci. Techol.*, vol. 49, pp. 79–92, 1986.

[34] D. S. Lee, K. D. Kihm, and S. H. Chung, "Analytical solutions for the developing jet from a fully-developed laminar tube flow," *J. Fluid Eng.*, vol. 119, pp. 716–718, 1997.

[35] R. W. Bilger, "The structure of turbulent nonpremixed flames," *Symp. (Int.) Combust.*, vol. 22, pp. 475–488, 1989.

[36] C. H. Gibson, "Fine structure of scalar fields mixed by turbulence. I. Zero-gradient points and minimal gradient surfaces," *Phys. Fluids*, vol. 11, p. 2305, 1968.

[37] C. S. Yoo, R. Sankaran, and J. H. Chen, "Three-dimensional direct numerical simulation of a turbulent lifted hydrogen jet flame in heated coflow: Flame stabilization and structure," *J. Fluid Mech.*, vol. 640, pp. 453–481, 2009.

[38] C. S. Yoo, E. S. Richardson, R. Sankaran, and J. H. Chen, "A DNS study on the stabilization mechanism of a turbulent lifted ethylene jet flame in highly-heated coflow," *Proc. Combust. Inst.*, vol. 33, pp. 1619–1627, 2011.

[39] H. S. Bak and C. S. Yoo, "Flame instabilities and flame cell dynamics in opposed nonpremixed tubular flames with radiative heat loss," *Combust. Flame*, vol. 194, pp. 322–333, 2018.

[40] K. S. Jung, S. O. Kim, S. H. Chung, and C. S. Yoo, "On the flame stabilization and stabilization characteristics of autoignited lainar lifted *n*-heptane jet flames in heated coflow air," *Combust. Flame*, vol. 223, pp. 307–319, 2021.

Acknowledgements

First of all, I would like to give my sincere gratitude to my advisor, Professor Chun Sang Yoo for directing my research and encouraging me during my master course. Owing to his persistent help, I could complete this thesis and have a chance to meet various fields. I also thank to my committee members-Professor Jae Hwa Lee and Professor Jooha Kim, for their valuable comments on my thesis.

I also express my thanks to all members of our laboratory for commenting this work in order to help me have various views. And 2 years I have spent together with my members in UNIST will be unforgettable.

In addition, I am always indebted to my family, whose countless supports make it possible for me to study hard. And finally, I am deeply appreciative of my husband, Kyu Ho Van, who is coworker of this study and the partner of my life. Without his love and inspiration, I would not achieve my academic goals.